The effect of confinement on dynamics and rheology of dilute deoxyribose nucleic acid solutions. II. Effective rheology and single chain dynamics

Nathanael J. Woo

Scientific Computing / Computational Mathematics Program, Stanford University, Stanford, California 94305

Eric S. G. Shaqfeh[a)]

Departments of Chemical and of Mechanical Engineering, Stanford University, Stanford, California 94305

Bamin Khomami

Department of Chemical Engineering and Materials Research Laboratory, Washington University, St. Louis, Missouri 63130

(Received 20 March 2003; final revision received 17 December 2003)

Synopsis

In this study we use the correct entropic spring force in the gap as discussed in Part I including hydrodynamic interactions with the wall to study the effect of confinement on deoxyribose nucleic acid rheology and chain dynamics. We present results for the chain density, the velocity, and the force density of the chains, which change rapidly over the length scale of the chain size. We associate this size and dynamics in these *near wall* layers to the configurational dispersion layer thickness δ_D found in polymer shear flow dynamics in the absence of the wall [Chopra and Larson (2002); Hur *et al.* (2000)]. Though such rapid variation in velocity and density profiles is localized near the wall, its effect on average mechanical properties is global and is felt even at large channel sizes beyond $20\,Rg$. We determine the effective viscosity of the dilute polymer solutions using self-consistent dynamics in these confined geometries and for large gap widths determine how the viscosity asymptotically approaches its bulk value. Finally, we also study the details of individual chain dynamics under confinement: This includes the tumbling motion of a chain in shear/Poiseuille flow, and relaxation from an extended state. We find that the confinement results in two different measures of the chain relaxation time: one shorter and the other longer than the longest relaxation time in the bulk. These two relaxation times are related to dynamics perpendicular and parallel to the walls, respectively. We show that different rheological experiments are sensitive to different specific relaxation times. © *2004 The Society of Rheology.* [DOI: 10.1122/1.1648643]

I. INTRODUCTION

In Part I of this series of communications [Woo *et al.* (2004)], we have shown that the presence of confining walls alters the random walk of the polymer chain near the boundaries in a planar channel, thereby changing its entropic spring force law. We have also

[a)]Author to whom all correspondence should be addressed; electronic mail: eric@chemeng.stanford.edu

found that the confinement increases the viscous drag on the chain, and to accomplish a correct description of the chain dynamics and the fluid rheology in the presence of confinement, it is necessary to correct the entropic spring force law and the viscous drag. In this communication we apply these findings to microchannel flows to study the rheology and chain dynamics of dilute deoxyribose nucleic acid (DNA) solutions in the presence of confining walls.

As shown in previous studies [Aubert and Tirrel (1982); Ausserre *et al.* (1991); Brunn (1976); Brunn and Grisafi (1987); Chopra and Larson (2002); Mavrantzas and Beris (1992); Muller-Mohnssen *et al.* (1990); Schiek and Shaqfeh (1995)], the main consequence of the confinement is that near the boundary, there exists a region called the *depletion layer* where chain segments are depleted due to the excluded volume interaction with the wall. Therefore, the chain concentration varies from zero at the wall to its bulk value over the length scale of this depletion layer. Clearly, the variation in concentration is coupled to variation in other quantities such as the force density and velocity profile. In this study, we have investigated the inter-relation between the depletion layer thickness and the configurational dispersion layer thickness in shear flow in the absence of confinement [Chopra and Larson (2002); Hur *et al.* (2000)]. Based on this investigation, we have developed the large gap width asymptotic scalings for the effective rheology of the dilute DNA solutions.

We have also investigated the chain tumbling dynamics both in the absence and presence of confinement via examining the appropriate autocorrelation and crosscorrelation of chain extension. By employing both Brownian dynamics simulations as well as analytical techniques we have elucidated the mechanisms involved in tumbling dynamics. We also endeavor to understand chain dynamics in confined geometries by examining the chain relaxation times. Specifically, it has been shown that the confinement splits the isotropic bulk relaxation time into two relaxation times: one perpendicular to the confining walls and the other parallel. These two relaxation times are closely related to tumbling chain dynamics in shear flow as well as to chain relaxation from an initially stretched configuration.

II. EFFECTIVE VISCOSITY

A. Definitions

To quantify the rheology of DNA solutions in thin channel shear flow we define the effective shear viscosity η^{eff} as the viscosity of the solution averaged over the gap width H:

$$\eta^{\text{eff}} = \frac{1}{H}\int_0^H \left[\eta_s + \frac{\langle \tau_{xy}^p(y)\rangle}{\dot{\gamma}}\right] dy, \tag{1}$$

where η_s is the Newtonian solvent viscosity and $\langle \tau_{xy}^p(y)\rangle$ is the ensemble average of nonlocal polymeric shear stress. Note that in the parallel plate geometry η^{eff} is equal to the ratio of the shear stress to the shear rate at the wall and therefore is the measurable viscosity in standard rheometry. For the case of Poiseuille flow, we define the effective viscosity as

$$\frac{\eta^{\text{eff}}}{\eta_s} = \frac{Q_{\text{Newtonian}}}{Q_{\text{non-Newtonian}}}, \tag{2}$$

where $Q_{\text{Newtonian}}$ is the volumetric flowrate in the absence of polymer (or DNA) present in the solution, and $Q_{\text{non-Newtonian}}$ is the flowrate with the polymer present.

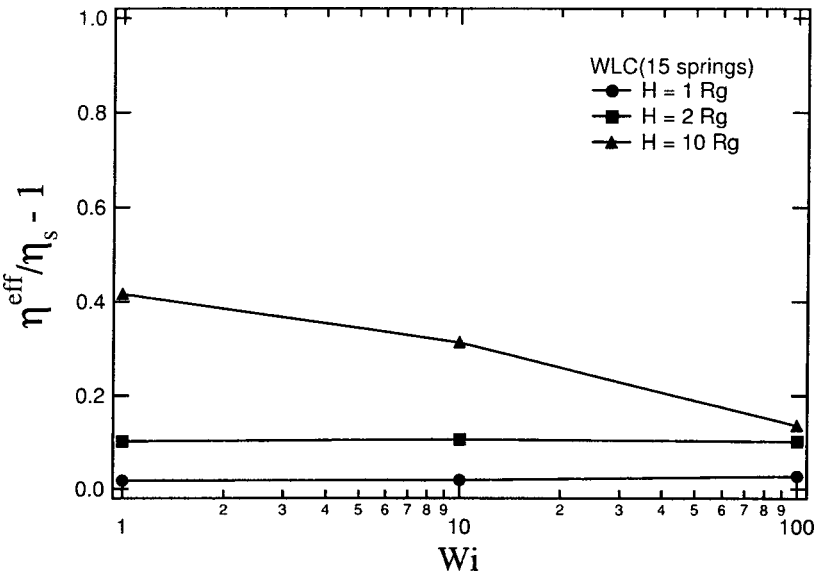

FIG. 1. The effective viscosity is independent of Wi at small gap width $H = 1\,Rg$. Only at large enough gap width, the effective viscosity is a function of Wi.

B. Narrow gap results [$H \ll O(Rg)$]

Two main factors that contribute to chain deformation in thin gap flows are the confining effect of the walls and the flow-induced deformation. In the absence of flow, due to the presence of the walls, a random walk in the direction perpendicular to the walls is greatly hindered, thus the chain is forced to spread in directions parallel to the walls. As the flow strength increases the chain resides in a small dispersion layer (δ_D or δ_2) which decreases in thickness as Wi increases [Hur *et al.* (2000)]. Therefore, under extreme confinement, the chain is already in a highly deformed state even without any flow and the effect of applying flow does not cause additional chain deformation except at high Wi (data corresponding to $H = 1\,Rg$ in Fig. 1). Therefore over a large Wi range, the effective viscosity, which is related to δ_D, is not a function of Wi but a function only of gap width H. Even though the extension in the direction perpendicular to the walls (δ_2 or δ_D) is nearly constant over a large Wi range [as shown by the collapse of data at different Wi for small H into one in Fig. 2(b)] for extreme confinement, the extension in the flow direction (L_1) remains a strong function of Wi [Fig. 2(a)]. Note in this context that shear thinning in the dispersion layer occurs at high Wi and thus δ_D is independent of Wi below a critical Wi (as is the shear viscosity). Chain extension in the flow direction (L_1), on the other hand, is a rapidly increasing function of Wi until it asymptotes to a constant value roughly half of the chain's contour length [Hur *et al.* (2000)].

Therefore, under extreme confinement, the effective viscosity is independent of Wi and is closely related to the zero shear viscosity of the chain (Fig. 1). Since the zero shear viscosity is proportional to the relaxation time, $\eta^{\text{eff}} - \eta_s$ scales as the relaxation time $\tau_\perp$ which is obtained from the zero-shear stress autocorrelation function in thin gap flows. The stress autocorrelation function will be discussed in detail in Sec. IV. In Fig. 3 we have plotted the relative effective viscosity at low Wi ($Wi = 1$) and it compares favorably with the normalized chain relaxation time in the thin gap. Also shown in the figure

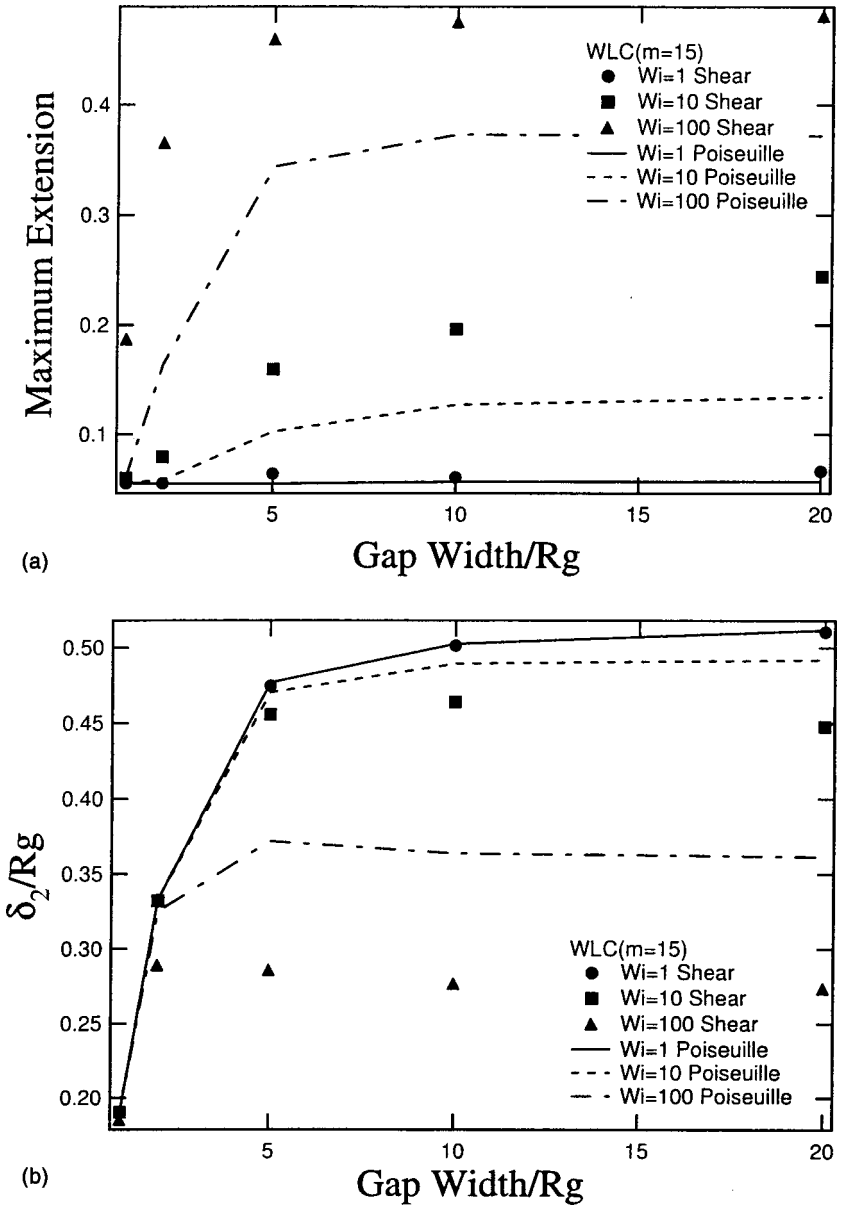

FIG. 2. Chain size vs gap width for λ-phage DNA [15 spring wormlike bead-spring chain (WLC)] at various Wi in both shear and Poiseuille flow. (a) Maximum chain extension in flow direction (L_1) and (b) chain extension in flow gradient direction (δ_2).

is the relaxation time estimate from the loss of configurational space volume due to confinement. This will be discussed in detail in Sec. IV as well.

C. Intermediate gap results [$H \sim O(Rg)$]

As the gap width increases, the relative importance of the effect of the confining wall decreases while the effect of the flow strength increases. In general the effective viscosity depends on both flow strength and the gap width at intermediate gap widths. Even though

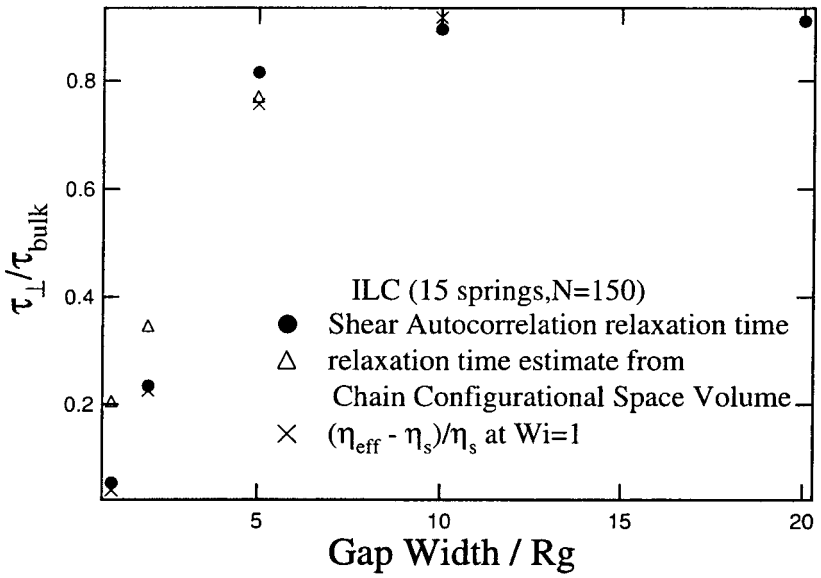

FIG. 3. Relaxation time based on autocorrelation of zero-shear stress as a function of gap width. Also shown are configurational volume estimate of the relaxation time and effective viscosity at $Wi = 1$.

the variations in chain density and force density are localized to regions near the walls, the effective viscosity is well below its asymptotic bulk value and the effect of the wall on the effective viscosity is still seen even at the gap widths of 20 Rg (Fig. 4). This effect is more pronounced at low flow strength where the dispersion layer thickness (δ_D) is largest and therefore the interaction of the chain with the wall is the greatest. A typical plot of the effective viscosity is shown in Fig. 4 as a function of flow strength.

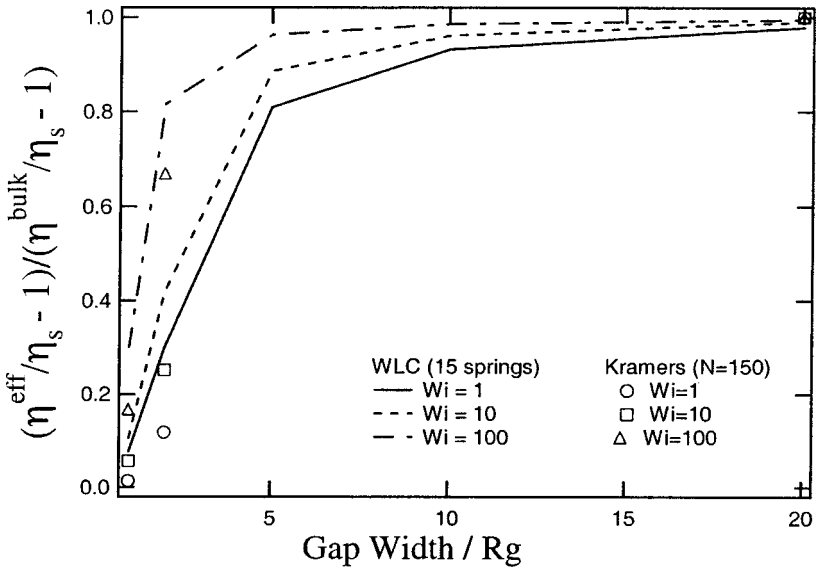

FIG. 4. Effective viscosity vs gap width for λ-phage DNA modeled by both WLC and bead-rod chain in shear flow.

Mavrantzas and Beris (1992) in their recent study added the effect of the wall on the Hookean probability distribution function and found that at higher shear rate the density profile *decreased* near the wall. This is in contrast to previous studies [Duering and Rabin (1990); Mavrantzas and Beris (1992)] including their own in which the density profile increased near the wall as the shear rate increased. In our *nonlocal* Brownian dynamics, we find the chain segmental density near the wall *increases* at higher shear rates. We have also performed *local* Brownian dynamics simulation to determine whether the discrepancy between our result and that of Mavrantzas and Beris (1992) is due to nonlinearity of the spring force or the *local* velocity field. In contrast to our *nonlocal* Brownian dynamics simulation results, in our *local* simulation, we find the chain density *decreases* near the wall. Therefore, the discrepancy between their finding and ours is not due to nonlinearity of the spring force law but is due to the *local* velocity field they used. In our more accurate *nonlocal* velocity field, near the wall the (*nonlocal*) shear rate is higher than the *local* shear rate. The chains are more extended in the flow direction [Fig. 2(a)] and less extended in the flow gradient direction [Fig. 2(b)] in the nonlocal flow field as compared to the local flow field. Therefore, if we consider a chain residing very near the wall, the chain's configurational space in the local flow field is *thicker* (i.e., δ_D is larger) in the flow gradient direction as compared to the chain's configurational space in the nonlocal flow field. It follows that the chain in the local field is repelled from the wall resulting in a lower chain segmental density profile near the wall. For nonlocal flow fields, the chain's configurational space is thinner (i.e., δ_D is smaller) and can approach the wall more readily, thus increasing the density profile near the wall.

D. Large gap asymptotic results [$H \gg O(Rg)$]

As we mentioned previously, near the wall, the chain and the force density profiles change rapidly over the length scale of the chain. However, in the region away from the wall these quantities remain constant. Moreover, our simulations clearly show that as the gap width is increased, these rapid variations near the wall remain of the same shape and in the limit of infinite gap width, the force density function can be treated as a *hat* function located near the wall (Fig. 5). Moreover, at sufficiently large gap widths, the details of the profile near the wall are not important and only the integral of this profile, which approaches a constant, is relevant. Thus, in order to develop an analytical relationship for the effective viscosity, the force density profile is approximated as a *hat* function as shown in Fig. 5. The momentum equation [Eq. (12) in Part I] is solved in the limit of large gap width H and one obtains the following expression for the effective viscosity:

$$\eta^{\text{eff}} \approx \eta^{\text{bulk}} - \eta^{p}\,\delta_D \frac{C_{\text{shear}}}{H}, \tag{3}$$

where C_{shear} is a constant independent of flow strength. We define the dispersion layer thickness δ_D (or δ_2) as

$$\delta_D = \sqrt{\frac{\Sigma_{\nu=1}^{N}\langle R_2^{\nu} R_2^{\nu}\rangle}{N}}, \tag{4}$$

where the summation is over the beads on the chain and R_2^{ν} is the y component of the bead position relative to its center of mass. Therefore, δ_D is just the y component of the radius of gyration. Note that unlike chains confined between two *narrow* walls ($H \sim O(Rg)$ in Fig. 2(b)], δ_2 does not change appreciably from its bulk value and bulk scaling and for large gap the chains can interact with only one wall. Since for flexible

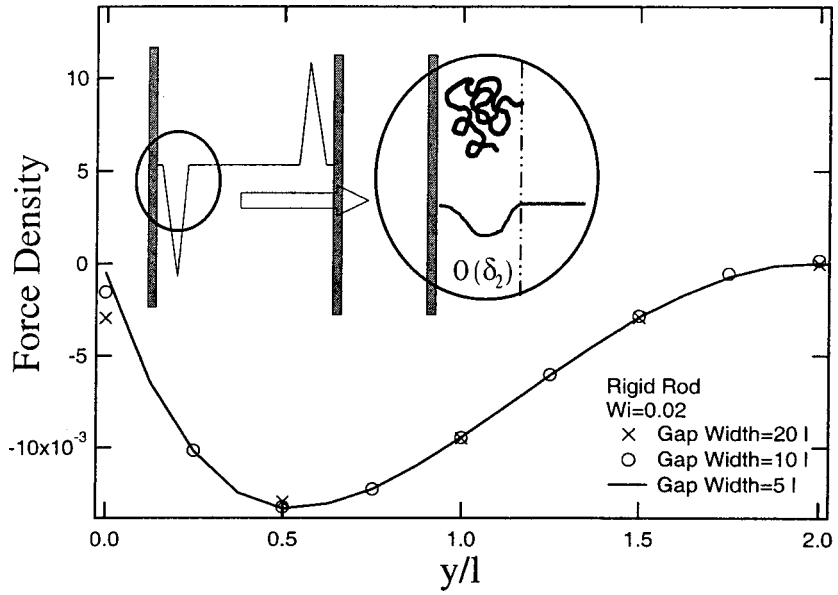

FIG. 5. Asymptotic force density profile near the wall for rigid rod suspensions. As the gap width is increased the profile tends to the asymptotic profile and becomes indistinguishable from it. Same applies to bead-spring and bead-rod chains (not shown). *l* denotes the half length of the rod. Detailed description of rod simulation can be found elsewhere [Woo (2003)]. For the insert figure: The force density profile can be approximated as two *hat* functions located near the walls. The region over which the force density is nonzero can be estimated by δ_2 and represented by a *hat* function.

chains, the polymeric contribution to shear viscosity (η^p) scales as $Wi^{-1/2}$ and the configurational dispersion layer (δ_D) scales as $Wi^{-1/4}$ [Hur *et al.* (2000)], from Eq. (3) we find $\Delta\eta^{\text{eff}}(=\eta^{\text{eff}}-\eta^{\text{bulk}})$ scales as $Wi^{-3/4}/H$ at large Wi. Note that the predictions of H and Wi dependence of the effective viscosity are consistent with full Brownian dynamics simulation results (Fig. 6). The inverse gap width dependence result is consistent with the rigid rod theory of Schiek and Shaqfeh (1995) and thus is applicable to both flexible and rigid chains. On the other hand, chains of different flexibilities clearly are characterized by a different Wi dependence of $\Delta\eta^{\text{eff}}$. $\Delta\eta^{\text{eff}}$ for flexible chains scales as $Wi^{-3/4}$ while for rigid rods scales as $Wi^{-1/2}$ due to different scalings for η^p.

A similar analysis can be carried out for Poiseuille flow. The expression for the effective viscosity becomes

$$\frac{1}{\eta^{\text{eff}}} \approx \frac{1}{\eta^{\text{bulk}}} - \left(\frac{1}{\eta^{\text{bulk}}} - \frac{1}{\eta_s}\right)\frac{C_{\text{poise}}}{H}. \tag{5}$$

Once again the inverse gap width dependence is observed.

III. SINGLE CHAIN DYNAMICS

A. Chain autocorrelations in thin gap flows

We have also examined single chain dynamics in the confined flows via examining the power spectral density (PSD) which is defined as the Fourier transform of the autocorrelation of the chain's end-to-end distance in the flow direction L_1, *viz.*

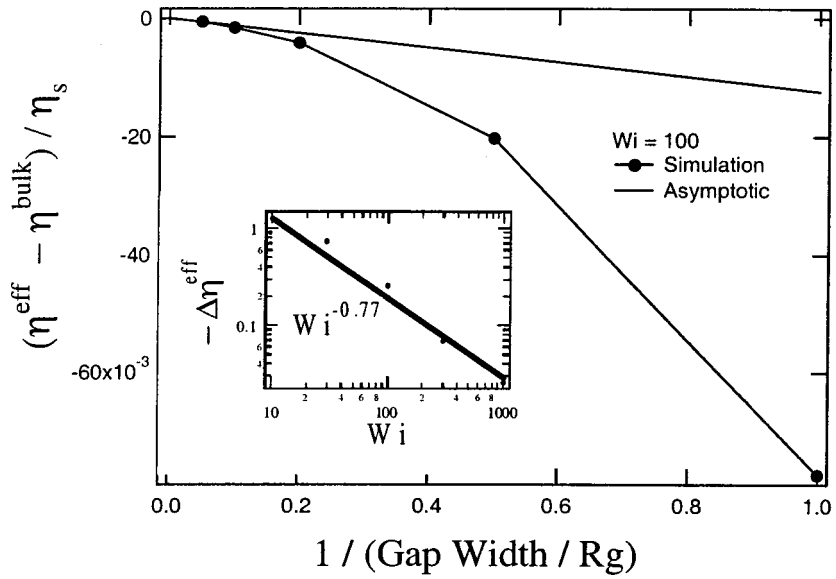

FIG. 6. Effective viscosity as a function of gap width at a large gap width. Inverse gap width dependence is observed at large gap width. For the insert figure: Effective viscosity as a function of Wi at a large gap width and large Wi at $c = 1$. Simulational scaling of $Wi^{-0.77}$ is close to the theoretical $Wi^{-3/4}$ scaling expected. The concentration is defined as $c = \xi^T n_p R g^3/\eta_s L$ where ξ^T is the viscous drag on the chain, n_p is the number density of the chain, L is the contour length of the chain, and η_s is the solvent viscosity.

$$\mathrm{PSD}(\omega) = \int_{-\infty}^{\infty} \langle L_1(t) L_1(0) \rangle e^{-i\omega t} dt. \tag{6}$$

Hur *et al.* (2000) studied the PSD of λ-phage DNA in three-dimensional (3D) bulk shear flow and found three distinct regions in the frequency domain: In the low frequency regime the PSD is found to be constant and thus independent of the frequency. At intermediate frequencies, the coupling of Browning fluctuations in the gradient direction and the convection in the flow direction causes the PSD to decay as $\omega^{-3.4}$. Finally, in the high frequency regime, the PSD decays as $\omega^{-1.6}$ and this region is due solely to Brownian fluctuations.

In our study, the presence of the chains and their associated extra stress creates a region of higher shear near the wall and a region of lower shear away from the wall. Since the chain segmental density is lower near the wall there are fewer chains undergoing tumbling at a faster rate than in the bulk. Also the presence of the wall reduces the dispersion layer size δ_D. Since tumbling results from the coupling of convection in the flow direction and Brownian fluctuations in the gradient direction, the effective magnitude of the convective velocity the chain samples is greatly reduced near the wall. This results in a hindered tumbling motion near the wall. Therefore, chains in the confined geometry undergo less tumbling in shear flows and are less extended than in the bulk. Shown in Fig. 7 are the PSDs of bead-spring models as calculated from Brownian dynamics simulation. As the gap width decreases, the chains are less extended as can be seen from the lower plateau of the PSD at low frequency and the coupling between the Brownian fluctuations and the shear flow is reduced as can be seen in the intermediate frequency region. The high frequency region is purely Brownian and is not affected by the confinement. As will be discussed in Sec. IV, a main consequence of confinement is

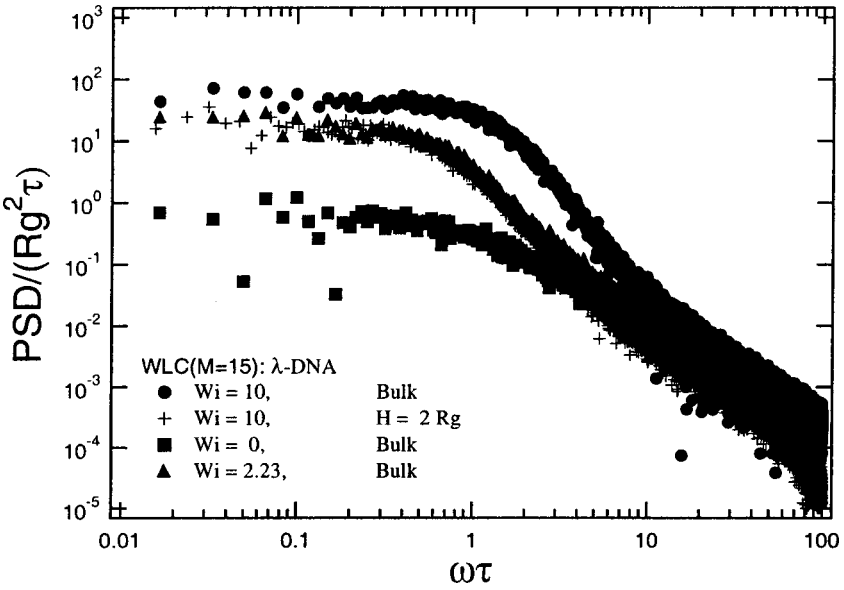

FIG. 7. PSD of bead-spring model. As the gap width decreases, tumbling motion is hindered. The reduction in chain relaxation time in thin gaps results in lower effective Wi and when this is taken into account, a good overlap between thin gap PSD and bulk PSD can be obtained.

to decrease the chain relaxation time $\tau_\perp$. Therefore, by rescaling the relaxation time of the PSD with the thin gap relaxation time $\tau_\perp$ (instead of the bulk relaxation time), we can obtain a perfect overlap between the thin gap PSD at gap width $H = 2Rg$ and $Wi = 10$ (which corresponds to $Wi^{\text{eff}} = 2.23$ due to the reduction in $\tau_\perp$) and the bulk PSD at $Wi = 2.23$ (Fig. 7).

For the case of Poiseuille flow, due to the symmetry of the velocity profile, we have three distinct characteristic regions as shown in Fig. 8. Near the wall, as in the shear flow case, the chains are depleted and we have less tumbling. Near the center of the channel we have a region of low shear where chains undergo no tumbling motion at all. Between these two regions, chains undergo tumbling motion in two different directions due to the sign change of the shear rate. To compare the PSD of Poiseuille flow to that of shear flow, one has to define the flow strength unambiguously in both cases. For the case of shear flow, the shear rate defined as the velocity gradient is constant everywhere across the gap for the case of Newtonian flow. But for Poiseuille flow the velocity gradient changes in the channel and there are different ways of defining the characteristic shear rate. Two common choices are the wall velocity gradient or the averaged velocity gradient over the gap. The former shear rate is twice the latter shear rate for the case of Newtonian flow. In this study we have investigated both choices and found the latter is a more meaningful shear rate for correlating tumbling dynamics of a single chain in Poiseuille flow. If we use the first definition of shear rate, we find the chains are less extended in Poiseuille flow than in shear flow, as signified by the lower plateau value at low frequencies in Fig. 8. No noticeable tumbling motion is present in Poiseuille flow at $Wi = 10$ between confined walls of $2\,Rg$, while there is considerable tumbling motion present in shear flow.

There are two main reasons for the drastic reduction in tumbling motion for the case of Poiseuille flow. The first reason is the *magnitude* of the local shear rate decreases near the center of the channel and thus the effective deformation that the chain experiences near the center of the channel is smaller. Hence, the chains undergo tumbling at a very

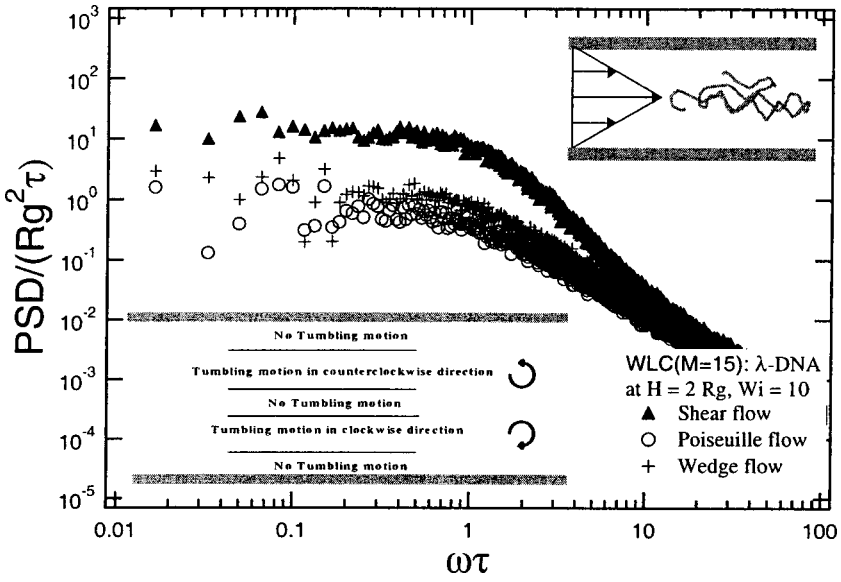

FIG. 8. Comparison of PSD for shear, Poiseuille and *wedge* flow at $Wi = 10$ and $H = 2\,Rg$. Less tumbling motion is observed in both Poiseuille and wedge flow compared to shear flow. For the upper insert figure: A schematic diagram for a *wedge* flow. Locally this is identical to shear flow except at the center where the shear rate changes sign. For the lower inset figure: Schematic diagram of regions where a chain can undergo tumbling motion in Poiseuille flow.

low effective shear rate. The second reason is the change of *sign* of velocity gradient in the center of the channel. We have carried out simulations of chain dynamics in a *wedge* flow as shown in Fig. 8. Even though the absolute magnitude of the local shear rate is the same for both shear and *wedge* flow, we find considerable reduction in the tumbling motion in *wedge* flow as also shown in Fig. 8. The important factor in chain tumbling dynamics is the average *signed* velocity gradient within the chain configurational dispersion layer. For a Poiseuille flow (and *wedge* flow) near the center of the channel, the region where the average velocity gradient is small can be bigger than the configurational dispersion layer due to the change in the sign of the shear rate and thus the chain effectively sees no *net* velocity gradient. Also the symmetry line in the center of the channel for a *wedge* flow can be thought of as an imaginary wall thereby reducing the *effective* gap width to half of the equivalent shear flow resulting in a reduced effective relaxation time. It follows that the type of flow can also further suppress the relaxation time scale of the chain dynamics in a thin gap. On the other hand, if we use the second definition for the shear rate to define Wi (i.e., defined in terms if the average velocity gradient across the gap), though the wall shear rate for the Poiseuille flow is twice that of the shear flow at the same Wi, we find on average that both shear and Poiseuille flow create chain tumbling at the same frequency and we find that the respective PSDs for the tumbling motion overlap perfectly as shown in Fig. 9.

B. Chain crosscorrelations in 3D bulk flows

To further elucidate the mechanism of chain tumbling dynamics in shear flow, we have also looked at the (*normalized*) cross-correlation function of the chain extensions in 1 and 2 Cartesian directions. The cross-correlation function is defined as

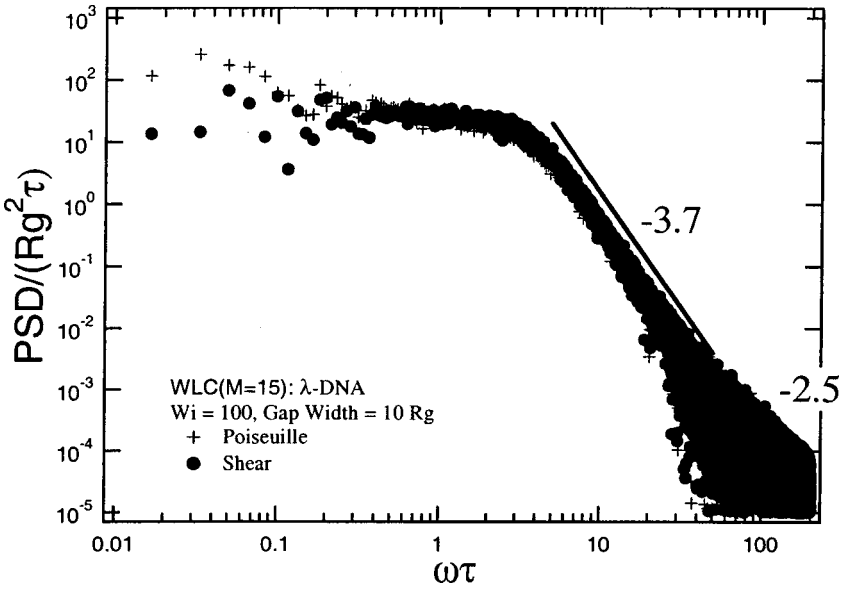

FIG. 9. PSD for shear and Poiseuille flow at $Wi = 100$ and $H = 10\,Rg$. When gap-averaged shear rate is used for Poiseuille flow, a good overlap with shear flow can be obtained.

$$C_{12}(T) = \frac{\langle R_2(t)R_1(t+T)\rangle}{\sqrt{\langle R_1(t)R_1(t)\rangle\langle R_2(t)R_2(t)\rangle}}, \tag{7}$$

where $\langle ... \rangle$ denotes an average over time t. First we consider the cross-correlation for linear and pre-averaged nonlinear chains in 3D bulk shear flow and then we will investigate the effect of confinement on full nonlinear chain dynamics.

The *normalized* cross-correlation function for FENE-P dumbbell is given by [Woo (2003)]:

$$C_{12}^{\text{FENE-P}}(T) = \frac{[1+TH(T)/\tau f]e^{-T/2\tau f}}{\sqrt{2+1/Wi^2 f^2}}, \tag{8}$$

where $H(T)$ is the heaviside function and $f\,(\equiv 1-\langle R^2\rangle/b)$ is the stiffness factor. Substituting $f = 1$ gives the Hookean dumbbell result. The stiffness factor f for the FENE-P can be determined by solving the following cubic equation, which arises from the closure of the FENE-P constitutive equation at steady state

$$L^{\text{FENE-P}}(f) = \left(\frac{2Wi^2}{3N}\right)f^3 + \left(1+\frac{1}{N}\right)f - 1 = 0. \tag{9}$$

Similarly one can obtain the cross correlation function for multi-spring models such as Rouse and FENE-PM model [Woo (2003)].

For FENE-P dumbbells, the effect of the nonlinear spring is taken into account by pre-averaging the nonlinear term in the spring force. This results in a stiffer spring at higher flow strength but the spring is still linear at any given flow strength.

We note that for linear spring models in shear flow, at high flow strength Wi, Eq. (8) with $f = 1$ becomes independent of Wi and $C_{12}(T)$ is positive for all time T. On the other hand, for pre-averaged nonlinear spring model FENE-P, the spring becomes stiffer

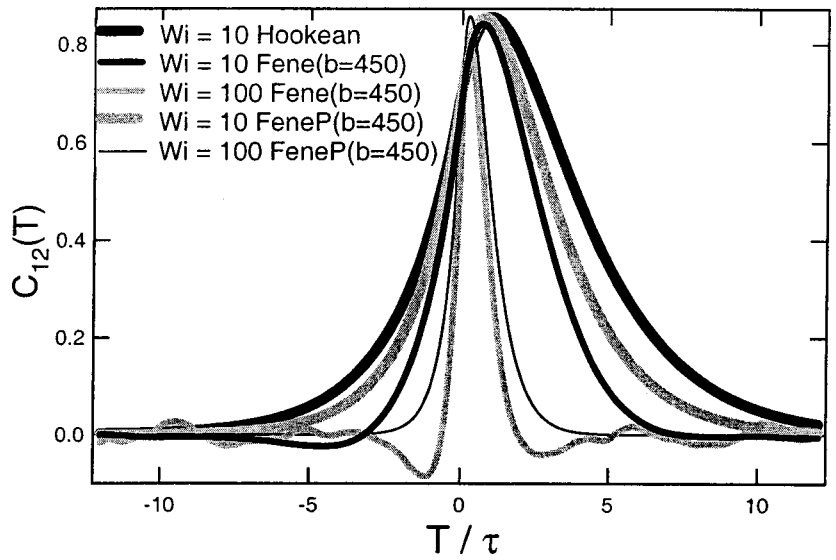

FIG. 10. The normalized cross-correlation function for linear and nonlinear spring models at various Wi.

at higher Wi and the correlation time becomes smaller due to the reduction in the stiffness factor f. However, the crosscorrelation remains positive for all time T for the FENE-P and linear spring. In contrast, recent Brownian dynamics simulations [Chopra and Larson (2002)] of nonlinear spring chains *without pre—averaging* show a negative valley both at positive and negative times at high values of Wi as shown in Fig. 10. Since linear spring chains which also undergo tumbling motion are characterized by no such negative valleys, the negative valleys are due to a *nonlinear coupling* of the spring forces in the flow direction and in the gradient direction. This *nonlinear coupling* results in the *thinning* and *thickening* of the chain configurational dispersion layer thickness (δ_2) during the tumbling cycle. Specifically the thinning process, which accompanies the stretching of the chain in the flow direction, gives rise to the negative valleys. As mentioned earlier for pre-averaged nonlinear spring models, at a constant Wi the spring is essentially linear with a different spring stiffness constant. Therefore, the dispersion layer thickness stays constant during the tumbling cycle. Hence, the pre-averaged models fail to give the negative valleys in the crosscorrelation. During the thinning cycle, the chain extends in the flow direction and *nonlinear coupling* of forces in the flow direction and flow gradient direction causes the chain to rotate toward the stagnation line resulting in a thinning of the chain configurational dispersion layer. During the thickening cycle, the chain contracts in the flow direction and the configurational dispersion layer thickens in flow gradient direction. The net effect of these thinning and thickening cycles is to rotate the chain in the same direction as the rotational component of the flow. Though pre-averaged nonlinear spring models fail to mimic this *additional rotation* due to the lack of any nonlinear coupling of the spring force, a minute amount of added vorticity to the applied shear flow makes the dynamics of even linear springs in qualitative agreement with our simulations of nonlinear chains since both a small amount of added vorticity and nonlinear coupling of spring force act to rotate the chain (Fig. 11).

We also find the cross-correlation function to be asymmetric in shear flow (Fig. 10). This is a signature of the nonzero vorticity in the flow. For purely extensional flow, the cross-correlation function is symmetric while for purely vortical flow the cross-

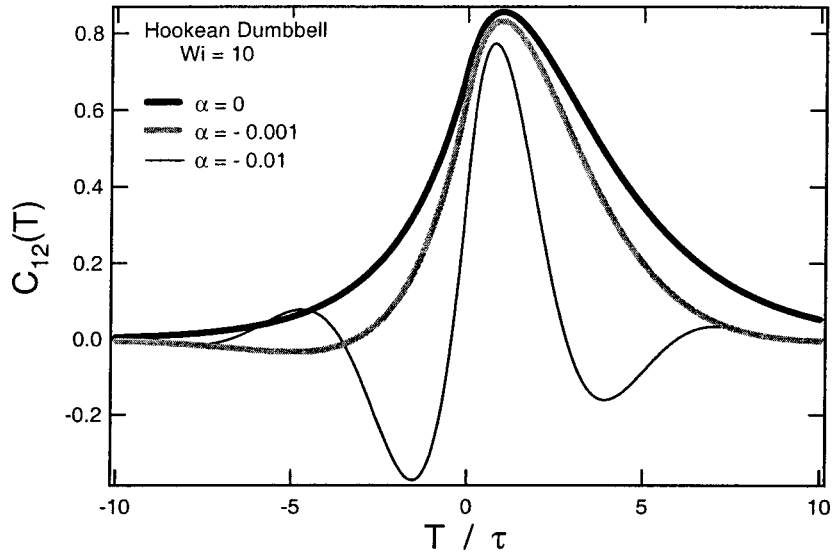

FIG. 11. The normalized cross-correlation function for Hookean Dumbbell at a given flow strength ($Wi = 10$) for various values of mixed flow parameter α ($\alpha = 0$ for shear flow). A minute amount of added vorticity to shear flow results in negative valleys as in nonlinear spring models.

correlation function is antisymmetric. A high positive correlation at a small positive time is due to the vortical component of the flow. For example, a large value of R_2 at a given time leads to a large value in R_1 at slightly later time resulting in a maximum in the crosscorrelation at a small positive time. The location of the negative valley at positive time is further removed from zero time than the location of the negative valley at negative time. This follows since the stretching cycle (or thinning cycle) occurs more slowly than the collapsing cycle (or thickening cycle) due to the opposing effect of the spring force to the convection during the stretching cycle.

C. Chain crosscorrelations in thin gap flows

As discussed in Sec. III A, chain confinement decreases the characteristic time scale governing chain tumbling dynamics. The time interval between the two negative valleys decreases as the gap width decreases as shown in Fig. 12. We also find the magnitude of the negative valley decreases under confinement. As Wi increases, the effect of the confining walls on chain deformation becomes smaller than the effect of flow strength and the difference between the crosscorrelation for bulk flows and the thin gap flows becomes smaller. On the other hand, the confinement effect is most strongly felt for small Wi since the configuration space of the chains is thicker in the flow gradient direction (i.e., δ_2 is larger) and therefore they interact more with the walls. At $Wi = 1$ the wall decorrelates R_1 and R_2 and suppresses the tumbling dynamics greatly reducing the chain extension in the flow direction.

IV. RELAXATION TIMES

It is also instructive to study the effect of confinement on the chain relaxation time in the thin gap. In 3D bulk problems, the relaxation time is isotropic since there is no preferred direction at equilibrium. But in a confined geometry, this symmetry is broken by the introduction of confining walls and one obtains different relaxation times for chain

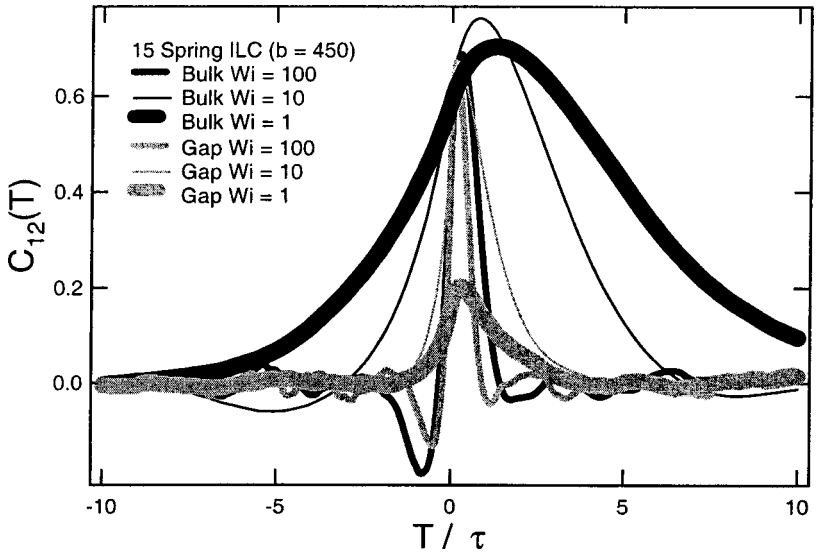

FIG. 12. The normalized cross-correlation function for λ-DNA chains under confinement ($H = 0.58\,Rg$) at various Wi.

deformation in different directions. For example, for flexible polymers, the longest relaxation time in the 3D bulk flow is given as $\tau_1 = \xi N^2/2\pi^2 H_{\rm sp}$, where ξ is the drag on a given bead, N is the number of beads, and $H_{\rm sp}$ is the spring constant [Bird *et al.* (1987)]. However, in the confined geometry, as shown in Part I, $H_{\rm sp}$ is different in different directions and the corresponding relaxation times differ from the bulk value τ_1. Here we denote the relaxation time in the direction *parallel* to the confining walls (xz plane) as $\tau_{\|}$ and the relaxation time in the direction *perpendicular* to the confining walls (y-coordinate direction) as $\tau_{\perp}$.

Shown in Fig. 13(a) is the relaxation time obtained from the autocorrelation of the shear stress as a function of gap width. The relaxation time is obtained by fitting the linear portion of the log plot of relaxation modulus $G_p(t)$ given by

$$G_p(t) = \langle \tau_{xy}^p(t)\tau_{xy}^p(0)\rangle_{\rm eq}, \tag{10}$$

where $\langle * \rangle_{\rm eq}$ represents the ensemble average with no flow.

As the gap width decreases, the relaxation time associated with the shear rheology and chain dynamics decreases from its bulk value to zero. This relaxation time is closely related to $\tau_{\perp}$ and its behavior can be understood in terms of the spring force in the direction *perpendicular* to the confining walls, $F_{\perp}$. As mentioned in Sec. III of Part I, as the gap width decreases, $F_{\perp}$ increases. Since the relaxation time scales as the inverse of the force, $\tau_{\perp}$ decreases as gap width decreases. The tumbling motion occurs in the xy plane, and the relevant relaxation time is that obtained from the auto correlation of shear stress τ_{xy}. Therefore, at a given shear rate, as the gap width decreases, the relaxation time decreases and the effective Wi decreases resulting in smaller chain deformations and extensions at a given flow strength. Rescaling the relaxation time of the PSD with the thin gap relaxation time $\tau_{\perp}$ instead of the bulk relaxation time, we obtain a perfect overlap between the thin gap PSD at gap width $H = 2Rg$ and $Wi = 10$ (which corresponds to $Wi^{\rm eff} = 2.23$ due to the reduction in $\tau_{\perp}$) and the bulk PSD at $Wi = 2.23$ (Fig. 7). A

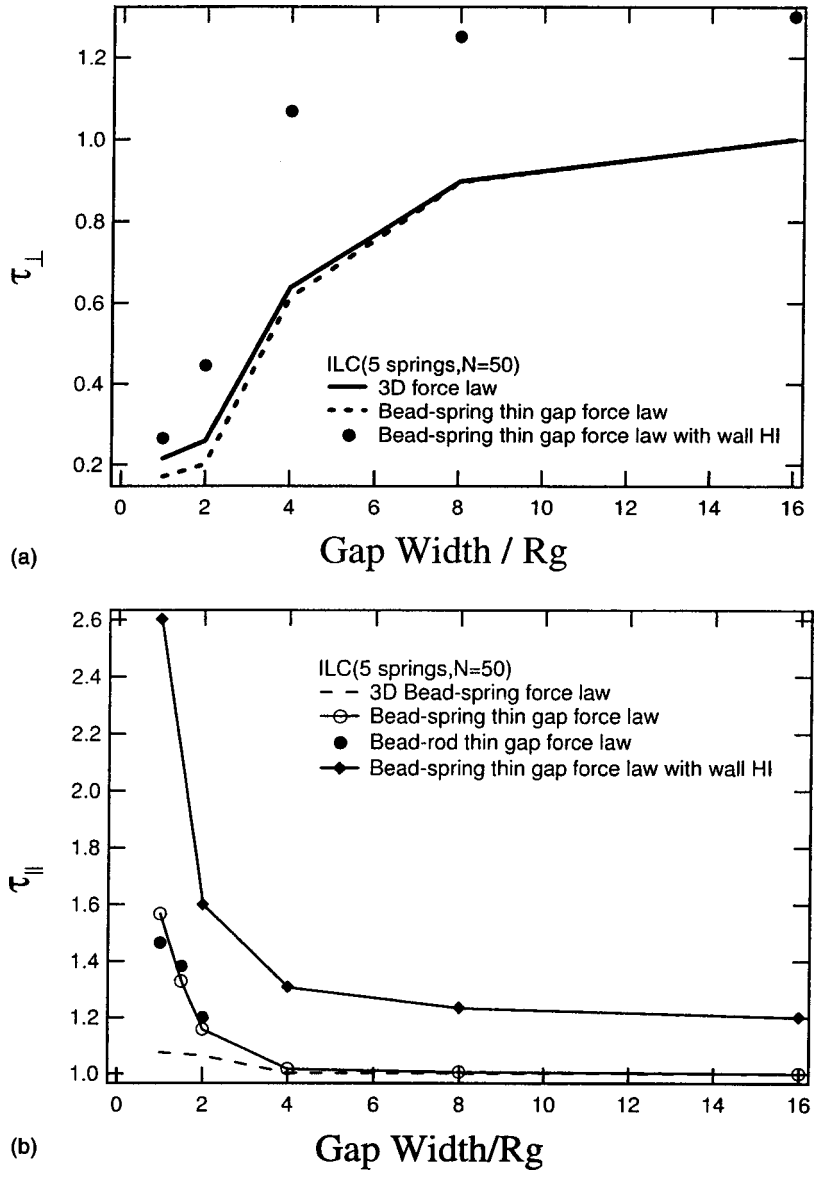

FIG. 13. The anisotropic relaxation times in confined geometry with and without wall HI is compared to the relaxation time based on uncorrected 3D force law. $\tau_\parallel$ and $\tau_\perp$ correspond to chain relaxation times parallel and perpendicular to the confining walls, respectively.

decrease in the relaxation time $\tau_\perp$ due to the confinement has also been observed for a suspension of rigid Brownian rods [Schiek and Shaqfeh (1995)].

Alternatively one can explain the decrease in relaxation time in terms of loss of configurational space under confinement [Schiek and Shaqfeh (1995)]. We define the configurational space volume as the product of three characteristic dimensions of the chain configurational space in each Cartesian coordinate in the absence of flow

$$V = \delta_1 \delta_2 \delta_3, \tag{11}$$

where δ_i is given by

$$\delta_i = \sqrt{\frac{\Sigma_{\nu=1}^{N}\langle (R_i^{\nu})^2\rangle}{N}}. \tag{12}$$

In the absence of the confining walls, the chain segments reside in a spherical coiled volume V^{sphere} at equilibrium. As the walls are brought in contact with the chain, the chain is compressed in the direction perpendicular to the confining walls and swells in the direction parallel to the walls. The new volume (V^{gap}) now occupied by the chain is greatly reduced compared to the 3D bulk configurational space. As a general rule of thumb, the greater the reduction in configurational space, the greater the change in relaxation time and the force law. In Fig. 3 we compare our estimate of the relaxation time from the ratio of the configurational space ($V^{\text{gap}}/V^{\text{sphere}}$) to the relaxation time $\tau_\perp$ obtained from the Brownian dynamics simulation of zero-shear stress auto correlation function [Eq. (10)] and a strong correlation is obtained. Also shown in Fig. 3 is the relative effective viscosity $[(\eta^{\text{eff}}-\eta_s)/\eta_s]$ at low Wi ($Wi = 1$). Under extreme confinement ($H \ll Rg$), as discussed in Sec. II B the flow cannot further deform the polymer chain relative to its equilibrium deformed conformation, hence, over a large Wi range, the effective viscosity is independent of Wi and is closely related to the zero shear viscosity of the chain (Fig. 1). Since the zero shear viscosity is proportional to the relaxation time, $\eta^{\text{eff}}-\eta_s$ scales as the relaxation time $\tau_\perp$. Therefore, the configurational volume can serve as a good estimate of the relaxation time $\tau_\perp$ and the relative effective viscosity in thin gaps.

On the other hand, for the case of relaxation from an elongated state (i.e., relaxation parallel to the walls) as in the experiment by Bakajin *et al.* (1998) where a chain is hooked on a post and elongated and subsequently allowed to relax, the relaxation time $\tau_\parallel$ can be determined from the decay of the normal stress difference, $N_1 = \tau_{xx} - \tau_{yy} \approx \tau_{xx}$. For small deformations, τ_{xx} can be approximated by $H_{\text{sp}}L_1^2$, where L_1 is the extension of the chain in the x direction (i.e., the direction in which the chain was originally elongated) and H_{sp} is the spring constant. In this case, unlike $\tau_\perp$, $\tau_\parallel$ increases due to confinement as shown in Fig. 13(b). As the chain retracts from its elongated high stress state to a coiled lower stress state, it bumps into the confining walls which impede the relaxation process resulting in larger relaxation times. In terms of the effective spring force law, the walls make the chains swell in the confinement plane exerting a force pushing the chains further away from equilibrium, resulting in a smaller effective restoring force. Therefore, confinement decreases the effective spring force in the direction parallel to the confining walls ($F_\parallel$) and its corresponding relaxation time ($\tau_\parallel$) increases.

It should be noted that good agreement for $\tau_\perp$ between the bead-spring model [for an inverse langevin chain (ILC) and the corresponding bead-rod model with the same number of Kuhn steps N is obtained [Fig. 13(b)]. When the wall HI is included, $\tau_\perp$ increases approximately 50% [Fig. 13(a)] while $\tau_\parallel$ increases by a factor of 2. Thus, in order to capture the physics correctly, it is crucial to include the effect of wall HI.

V. HYDRODYNAMIC INTERACTIONS WITH THE WALL

In Part I we have shown the importance of *wall HI* for chain relaxation from an extended state in confined geometries. In this section we study its effect on chain tumbling dynamics. For the tumbling dynamics of chains in shear and Poiseuille flow, there is a coupling of Brownian motion in the flow gradient direction and the convection in the flow direction. The drag coefficients are different in directions parallel and perpendicular to the wall as shown in Sec. V of Part I. To guide our understanding of chain dynamics

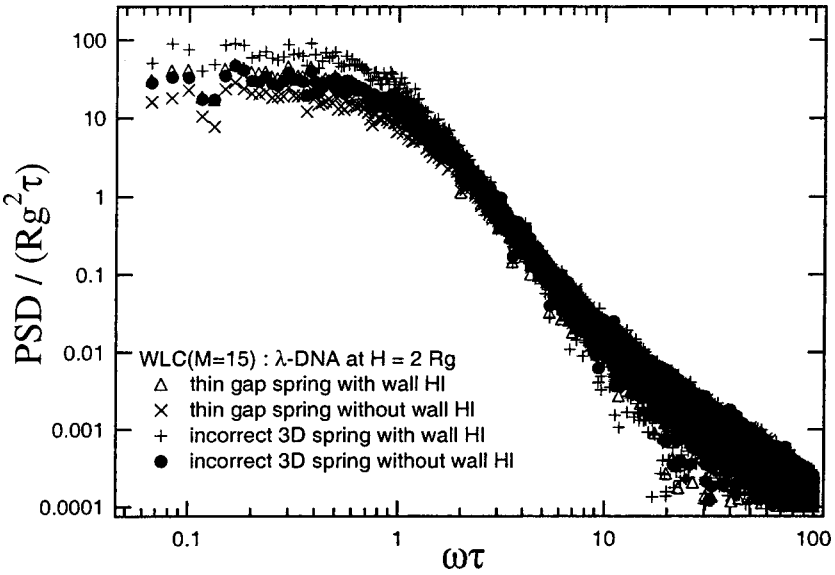

FIG. 14. PSD for 15 spring ILC corresponding to λ-phage DNA ($N = 150$).

in thin gaps, we again use the Hookean dumbbell model to obtain an analytical expression for the PSD of a chain in shear flow with *anisotropic* drag. In this context, Hur *et al.* (2000) showed that the qualitative behavior of the chain tumbling dynamics for nonlinear bead-spring models could be captured successfully using the linear Hookean dumbbell model. In the Fourier space, the equation $\hat{R}_1(\omega)$ for a Hookean dumbbell with anisotropic drag can be written as

$$\hat{R}_1(\omega) = \frac{\hat{F}_1^{\mathrm{Br}}(\omega)}{\xi\left(\frac{1}{2\tau} - i\omega\beta_{\parallel}\right)} + \frac{\hat{F}_2^{\mathrm{Br}}(\omega)\,\dot{\gamma}\beta_{\parallel}}{\xi\beta_{\perp}\left(\frac{1}{2\tau} - i\omega\beta_{\perp}\right)\left(\frac{1}{2\tau} - i\omega\beta_{\parallel}\right)}, \tag{13}$$

where $\hat{R}_i(\omega)$ and $\hat{F}_i^{\mathrm{Br}}(\omega)$ are the Fourier transform of the Hookean dumbbell length and Brownian force on the bead in the ith coordinate direction, respectively. $\beta_{\parallel}\xi$ and $\beta_{\perp}\xi$ are the anisotropic drag coefficients in directions parallel and perpendicular to the walls, respectively. For the case of $\beta_{\parallel} = \beta_{\perp} = 1$, we recover the isotropic drag result. To simplify our analysis, we assume the drag coefficients are constant over the gap width and thus use the weighted average drag coefficients from Eq. (21) in Part I. Then from Eq. (13), we obtain the PSD for the Hookean dumbbell with an anisotropic drag

$$\mathrm{PSD}(\omega) = \frac{16kT\tau^2\langle\beta_{\parallel}\rangle}{\xi}\left[\frac{1}{1+(2\tau\langle\beta_{\parallel}\rangle\omega)^2}\right]\left[1+\frac{4Wi^2\langle\beta_{\perp}\rangle\langle\beta_{\parallel}\rangle}{1+(2\tau\langle\beta_{\perp}\rangle\omega)^2}\right]. \tag{14}$$

Clearly as the confining walls are brought together, the drag coefficient increases due to hydrodynamic interaction with the wall. Hence, the PSD increases in comparison to the PSD without wall HI especially in the low frequency regime compared to the PSD without the wall HI. This is confirmed in our simulation as shown in Fig. 14, where we compare the PSDs of a bead-spring chain with and without the wall HI for λ-phage DNA at gap width of $2\,Rg$. On the other hand if we compare the PSD for a chain using the 3D spring force law to the PSD using the thin gap force law, the PSD for a chain with the 3D

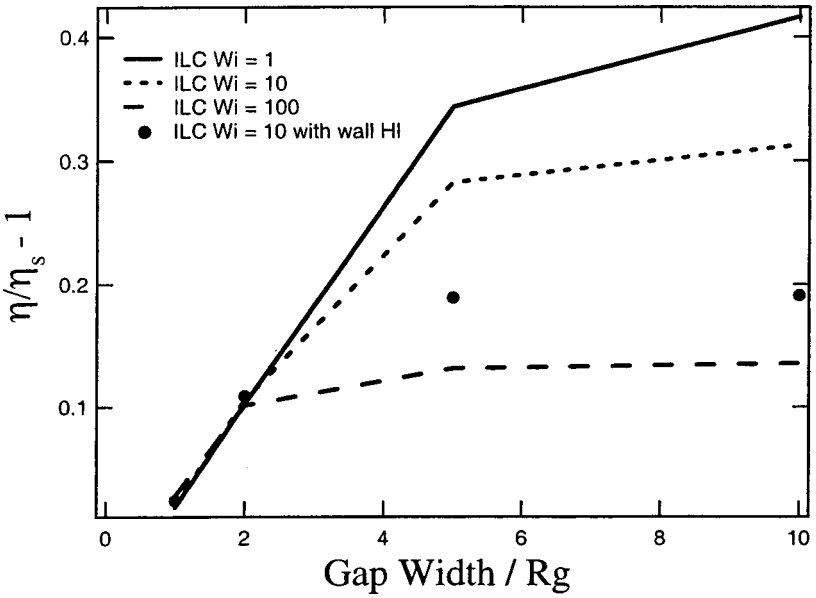

FIG. 15. Effective viscosity vs gap width at various Wi for 15 spring ILC corresponding to λ-phage DNA ($N = 150$).

spring force law is larger than that of the thin gap. Therefore, the use of the incorrect 3D force law overpredicts the PSD, while neglecting the wall HI underpredicts the PSD. Hence, a comparison of the PSD of the correct thin gap force law with wall HI to the PSD of incorrect 3D force law without wall HI, shows a reasonable agreement due to cancellation of errors (Fig. 14). It should be noted that the favorable comparison is only coincidental. In fact, as shown in Part I, the relaxation of a chain from a stretched state can only be captured when both the correct spring force law and the wall HI are taken into consideration.

The expression inside the second bracket [ ] of Eq. (14) suggests that $\sqrt{\langle\beta_\perp\rangle\langle\beta_\parallel\rangle}Wi$ is the effective flow strength induced by *drag increase*. Note that in derivation of Eq. (14), we did not take the modification of the spring force in thin gaps into account. Therefore, in general, the effective flow strength for thin gap flows can be defined as $Wi^{\text{eff}} = \sqrt{\langle\beta_\perp\rangle\langle\beta_\parallel\rangle}(\tau_\perp/\tau_{\text{bulk}})\,Wi$. The term $\tau_\perp/\tau_{\text{bulk}}$ accounts for the modification of spring force laws in thin gaps and the term $\sqrt{\langle\beta_\perp\rangle\langle\beta_\parallel\rangle}$ accounts for the increase in drag. Since $\sqrt{\langle\beta_\perp\rangle\langle\beta_\parallel\rangle}$ is always greater than unity, the dumbbell experiences a higher effective deformation at a given flow strength. Therefore, at large gap widths (where $\tau_\perp/\tau_{\text{bulk}}$ is nearly unity), due to the increase in drag on the chain, the effective viscosity *with* wall HI lies below the curve for the effective viscosity *without* HI due to shear-thinning effects at a higher effective shear rate (Fig. 15). But at smaller gap widths, the chain relaxation time ($\tau_\perp$) decreases significantly, therefore, we have very small effective flow strength at small gap widths. As shown in Sec. II B, the flow has very little effect on chain deformation beyond the deformation caused by confinement, thus, the effective viscosity is not a function of Wi and the effective viscosities at different Wi overlap. The effective viscosity with wall HI is slightly above the curve for the effective viscosity without the wall HI due to the term $\sqrt{\langle\beta_\perp\rangle\langle\beta_\parallel\rangle}$ which makes the DNA solution more viscous.

VI. CONCLUSIONS

In this study we have investigated the chain dynamics and the rheology of dilute DNA solutions in the presence of confining walls using both bead-rod and bead-spring models. We solved the self-consistent momentum equation that takes the effect of chain deformation on the flow velocity into account. Near the wall there is a depletion layer where the velocity, the chain density and the force density change rapidly over the length scale of the chain. Though the size of the dispersion layer is small, its effect is felt even beyond a gap width of $20\,Rg$. For small gap widths ($H \ll Rg$), the effective viscosity is only a function of gap width and is independent of flow strength. Therefore, the effective viscosity can be expressed in terms of the relaxation time obtained from the zero-shear stress autocorrelation, or configurational space volume estimate. For large channel sizes, the rheology of the confined system can be characterized in terms of its bulk properties such as the polymeric viscosity η^p and the dispersion layer thickness δ_D and $\eta^{\text{eff}} - \eta^{\text{bulk}}$ was found to scale as $Wi^{-3/4}/H$ for flexible polymers.

We have also investigated the tumbling motion of the chain via the PSD. The wall affects the coupling between the convective motion and the Brownian fluctuation appreciably, resulting in a slower tumbling motion of the chain as compared to tumbling motion in the bulk. Such a change in chain dynamics under confinement is linked to a reduction of the effective chain relaxation time, which results in smaller chain deformation at a given shear rate. Though chains undergo very different tumbling motions in Poiseuille and shear flow, on average the chains undergo the same degree of tumbling motion when compared at the appropriately chosen flow strength (i.e., the gap averaged shear rate). We have also further elucidated the mechanism of chain tumbling motion via examining the cross-correlation function. In shear flow, chains undergo a continuous cycle of thinning and thickening of the dispersion layer in the gradient direction. This results in negative valleys in the cross-correlation function and these are a signature of the nonlinear coupling of the force, i.e., the negative valleys are not captured by linear or pre-averaged nonlinear chain models.

Though the relaxation time associated with tumbling motion decreases under confinement, the relaxation time associated with the relaxation of chain length from an extended state increases. This is closely related to the symmetry breaking of the force under confinement. In the tumbling dynamics, the chains undergo tumbling motion in the plane perpendicular to the walls and therefore confinement results in faster dynamics due to an increase in the force perpendicular to the confining walls. On the other hand, for the relaxation of a chain from an extended state, the chains retract to their coiled state in the plane parallel to the confining walls. The spring force in this plane is lowered by confinement and therefore the relaxation process is slower.

ACKNOWLEDGMENTS

E.S.G.S. and B.K. would like to thank the National Science Foundation for supporting this work through Grant. Nos. CTS-9731896-002 and CTS-97325535, respectively.

References

Aubert, J. H., and M. Tirrel, ''Effective viscosity of dilute polymer solutions near confining boundaries,'' J. Chem. Phys. **77**, 553–561 (1982).

Ausserre, D., J. Edwards, J. Lecourtier, H. Hervet, and F. Rondelez, ''Hydrodynamic thickening of depletion layers in colloidal solutions,'' Europhys. Lett. **14**, 33–38 (1991).

Bird, R. B., C. F. Curtiss, R. C. Armstrong, and O. Hassager, *Dynamics of Polymeric Liquids, Vol. 2, Kinetic Theory* (Wiley, New York, 1987).

Brunn, P. O., ''The effect of a solid wall for the flow of dilute macromolecular solutions,'' Rheol. Acta **15**, 23–29 (1976).

Brunn, P. O., and S. Grisafi, ''Wall effects in simple shear of dilute polymer solutions: Exact results for very narrow and very wide channels,'' J. Non-Newtonian Fluid Mech. **24**, 343–363 (1987).

Chopra, M., and R. G. Larson, ''Brownian dynamics simulations of isolated polymer molecules in shear flow near adsorbing and nonadsorbing surfaces,'' J. Rheol. **46**, 831–862 (2002).

Duering, E., and Y. Rabin, ''Polymers in shear flow near repulsive boundaries,'' Macromolecules **23**, 2232–2237 (1990).

Hur, J. S., E. S. G. Shaqfeh, and R. G. Larson, ''Brownian dynamics simulations of single DNA molecules in shear flow,'' J. Rheol. **44**, 713–742 (2000).

Mavrantzas, V. G., and A. N. Beris, ''Theoretical study of wall effects on the rheology of dilute polymer solutions,'' J. Rheol. **36**, 175–213 (1992).

Muller-Mohnssen, H., D. Weiss, and A. Tippe, ''Concentration dependent changes of apparent slip in polymer solution flow,'' J. Rheol. **34**, 223–244 (1990).

Schiek, R. L., and E. S. G. Shaqfeh, ''A nonlocal theory for stress in bound, Brownian suspensions of slender, rigid fibres,'' J. Fluid Mech. **296**, 271–324 (1995).

Woo, J. H., *DNA chain dynamics and its applications to micro-devices and scission*, Ph.D. thesis, Stanford University (2003).

Woo, N. J., E. S. G. Shaqfeh, and B. Khomami, ''Effect of confinement on dynamics and rheology of dilute DNA solutions. I. Entropic spring force under confinement and a numerical algorithm,'' J. Rheol. **48**, 281 (2004).